Biodegradable PEG-poly(ω-pentadecalactone- co - p -dioxanone) nanoparticles for enhanced and sustained drug delivery to treat brain tumors

Published in final edited form as:
Biomaterials. 2018 September ; 178: 193–203. doi:10.1016/j.biomaterials.2018.06.024.

Biodegradable PEG-poly(ω-pentadecalactone-*co*-*p*-dioxanone) Nanoparticles for Enhanced and Sustained Drug Delivery to Treat Brain Tumors

Evan M. Chen[a], **Amanda R. Quijano**[a], **Young-Eun Seo**[a], **Christopher Jackson**[b], **Alexander D. Josowitz**[a], **Seth Noorbakhsh**[b], **Andrea Merlettini**[c], **Ranjini K. Sundaram**[b], **Maria Letizia Focarete**[c], **Zhaozhong Jiang**[d], **Ranjit S. Bindra**[b], and **W. Mark Saltzman**[a,#]

[a]Department of Biomedical Engineering, Yale University, New Haven, CT 06511, USA

[b]Department of Therapeutic Radiology, Yale School of Medicine, New Haven, CT, 06511, USA

[c]Department of Chemistry “G. Ciamician” and INSTM UdR of Bologna, University of Bologna, 40126 Bologna, Italy

[d]Department of Biomedical Engineering, Yale University, West Haven, CT 06516, USA

Abstract

Intracranial delivery of therapeutic agents is limited by penetration beyond the blood-brain barrier (BBB) and rapid metabolism of the drugs that are delivered. Convection-enhanced delivery (CED) of drug-loaded nanoparticles (NPs) provides for local administration, control of distribution, and sustained drug release. While some investigators have shown that repeated CED procedures are possible, longer periods of sustained release could eliminate the need for repeated infusions, which would enhance safety and translatability of the approach. Here, we demonstrate that nanoparticles formed from poly(ethylene glycol)-poly(ω-pentadecalactone-*co*-*p*-dioxanone) block copolymers [PEG-poly(PDL-*co*-DO)] are highly efficient nanocarriers that provide long-term release: small nanoparticles (less than 100 nm in diameter) continuously released a radiosensitizer (VE822) over a period of several weeks *in vitro*, provided widespread intracranial drug distribution during CED, and yielded significant drug retention within the brain for over 1 week. One advantage of PEG-poly(PDL-*co*-DO) nanoparticles is that hydrophobicity can be tuned by adjusting the ratio of hydrophobic PDL to hydrophilic DO monomers, thus making it possible to achieve a wide range of drug release rate and drug distribution profile. When administered by CED to rats with

[#]Correspondence should be addressed to W. Mark Saltzman: Department of Biomedical Engineering, Malone Engineering Center, Yale University, 55 Prospect Street, New Haven, CT 06511 USA. Tel: (203) 432-4262. mark.saltzman@yale.edu.

Conflict of Interest
The authors declare no conflict of interest.

Supplementary Data
The following supplementary data related to this article is available:
Table S1
Figs. S1, S2, S3, S4
Reference S1

intracranial RG2 tumors, and combined with a 5-day course of fractionated radiation therapy, VE822-loaded PEG-poly(PDL-*co*-DO) NPs significantly prolonged survival when compared to free VE822. Thus, PEG-poly(PDL-*co*-DO) NPs represent a new type of versatile nanocarrier system with potential for sustained intracranial delivery of therapeutic agents to treat brain tumors.

Keywords

Nanoparticles; Convection-enhanced delivery; PEG; Radiosensitizer; Intracranial

1. Introduction

Over the past decade, advances in cancer nanotechnology have allowed delivery of therapeutic agents to tumors with significantly decreased systemic toxicity [1–3]. When administered systemically, nanoparticle (NP)-based drug delivery systems can protect encapsulated therapeutic agents from rapid clearance through enzymatic digestion, renal filtration, or phagocytosis by the reticuloendothelial system [4, 5]. Further, those nanoparticles with their surfaces modified by hydrophilic polymers such as poly(ethylene glycol) (PEG) or hyperbranched polyglycerols (HPG) have low tendency to form aggregates and reduced uptake by phagocytes, further prolonging their circulation times and retention at targeted sites [6–8]. Nevertheless, sustained release of encapsulated agents is difficult to achieve in most NP formulations: usually, the size of particles must be greater than 300–400 nm to be capable of releasing drug at controlled rates for more than one week [9–11]. But some applications require smaller particles; NPs with diameters smaller than 100 nm that provide low bursts and sustained release could enable new clinical applications.

Previously, attempts to use nanomaterials for delivery of therapeutic agents into the brain have largely been stymied by the blood-brain barrier (BBB) [12, 13]. Even particles modified to enhance penetration through the BBB have <1% of injected dose reaching the brain tissue after systemic administration [14–16]. But drugs can be administered directly to the brain by infusion in fluids. For example, in convection-enhanced delivery (CED), fluid is introduced into the brain via trans-cranial catheters; fluid infusion is controlled by a hydrostatic pressure gradient [17]. CED can be safely performed in humans [18], but one of the major challenges with CED is that most drugs disappear from the brain quickly after the end of the infusion period [19]. To extend the period of treatment after a CED infusion, suspensions of sustained release NPs have been infused into the brain [20, 21]. CED of NPs to treat brain tumors is improved with NPs < 100 nm in diameter, because of their enhanced penetration through the brain parenchyma compared to larger particles [21]. The introduction of PEG surface coatings may also enhance the distribution of NPs after CED [22], although size appears to be a more important factor than surface chemistry in determining the volume of distribution during NP CED [23].

Poly(ω-pentadecalactone-*co*-*p*-dioxanone) [poly(PDL-*co*-DO)] is a family of biocompatible and biodegradable copolyesters that can be formed into NPs [24]. Previous studies show that the copolymers degrade hydrolytically under physiological conditions at controlled rates over a period of several months due to their unique isodimorphic properties and random

distribution of ω-pentadecalactone (PDL) and p-dioxanone (DO) repeat units in the polymer chains [25]. Modulation of the copolymer composition is an effective means to tune drug release rates from poly(PDL-*co*-DO) NPs [24]. Although the poly(PDL-*co*-DO) NPs are capable of delivering agents at sustained rates, formulations described thus far yield NPs with diameters of 200–400 nm, which produce small volumes of distribution when administered by CED [26].

Here, we tested the hypothesis that conjugation of PEG to poly(PDL-*co*-DO) chains would yield PEG-poly(PDL-*co*-DO) block copolymers that can be formulated into small nanoparticles (< 100 nm) with two key properties for intracranial drug delivery: penetration to large volumes when administered by CED and release of drugs over long periods. We found that PEG-poly(PDL-*co*-DO) NPs release hydrophobic therapeutic agents over a period of more than 28 days *in vitro* and penetrate in the brain tissues of rats after CED. To show that these properties enhance the treatment of intracranial tumors, PEG-poly(PDL-*co*-DO) NPs encapsulating an inhibitor of the ataxia telangiectasia-related (ATR) protein and known radiosensitizer, VE822, were administered by CED to rats with intracranial tumors [27]. A single infusion of VE822 NPs improved survival of animals receiving fractionated radiotherapy. PEG-poly(PDL-*co*-DO) copolymers are new materials with potential to improve the delivery of potent agents for treating brain tumors.

2. Materials and Methods

2.1. Materials

ω-Pentadecalactone (PDL), poly(ethylene glycol) methyl ether (M_n = 2000 Da, MeO-PEG2K-OH), and Novozym 435 catalyst (*Candida antarctica* lipase B or CALB supported on acrylic resin) were obtained from Sigma-Aldrich Chemical. The enzyme catalyst was dried at 40 °C under 2.0 mmHg overnight prior to use. *p*-Dioxanone (DO) was acquired from Leap Labchem Scientific Co. in China. Aceonitrile and dimethylsulfoxide were obtained from J.T. Baker (Avantor Performance Materials, Central Valley, PA, USA). VE822 was obtained from Selleck (Houston, TX, USA). DiI dye was purchased from Thermo Fisher Scientific (Waltham, MA, USA). RG2 cells were purchased from ATCC (Manassas, VA). Normal Human Astrocytes were obtained from Tim Chan at Memorial Sloan Kettering Cancer Center. All cells were cultured in 5% CO2 and air humidified in a 37 °C incubator. Each cell line was cultured up to passage number 20.

2.2. Enzymatic synthesis of PEG-poly(PDL-*co*-DO) diblock copolymers

The reaction substrates, ω-pentadecalactone (PDL), *p*-dioxanone (DO) and poly(ethylene glycol) methyl ether (M_n = 2000 Da, MeO-PEG2K-OH) in various ratios (Table 1), were blended with Novozym 435 catalyst (5 wt% vs total substrate) and toluene solvent (200 wt% vs total substrate). The resultant mixtures were stirred at 70 °C under atmospheric nitrogen gas for 26 h. At the end of the reactions, *n*-hexane was added to the product mixtures to cause precipitation of the formed copolymers. The crude polymers were washed with *n*-hexane twice and then dissolved in chloroform. After filtration to remove the catalyst particles, the polymer solutions were dropwise added to *n*-hexane to re-precipitate the PEG-poly(PDL-*co*-DO) copolymers. Finally, the block copolymers were washed with *n*-hexane

and dried under high vacuum (< 1.0 mmHg) at 40 °C overnight. The structure and composition of the polymers were analyzed by both proton and carbon-13 NMR spectroscopy using an Agilent 500 spectrometer, and their molecular weights and polydispersity values were measured by gel permeation chromatography (GPC) in chloroform using polystyrene standards. Non-PEGylated poly(PDL-*co*-DO) copolymer was produced by an identical method, but without the addition of the poly(ethylene glycol) methyl ether.

PEG-poly(PDL-*co*-DO): (a) ^{1}H-NMR ($CDCl_3$) (ppm) - *PDL units*: 4.05–4.13 (m, -CH_2-CH_2-$(CH_2)_{10}$-CH_2-CH_2-COO-), 2.27–2.36 (m), 1.61 (m), 1.26 (br.,); *DO units*: 4.36/4.27 (br., -CH_2-CH_2-O-CH_2-COO-), 4.13–4.19 (m, -CH_2-CH_2-O-CH_2-COO-), 3.79 (br.); *EO units*: 3.65; plus a small peak at 3.38 due to terminal –OCH_3 groups. (b) Selected ^{13}C NMR absorptions ($CDCl_3$) (ppm): 174.0 (PDL-PDL*-PDL/DO-PDL*-PDL, -CH_2-CH_2-$(CH_2)_{10}$-CH_2-CH_2-*C*OO-), 173.8 (PDL-PDL*-DO/DO-PDL*-DO, -CH_2-CH_2-$(CH_2)_{10}$-CH_2-CH_2-*C*OO-), 170.2, 170.1, 170.0 (PDL-DO*-PDL, PDL-DO*-DO/DO-DO*-PDL, DO-DO*-DO, -CH_2-CH_2-O-CH_2-*C*OO-), 70.55 (-*C*H_2-*C*H_2-O-), 69.6/69.2 (-*C*H_2-CH_2-O-CH_2-COO-), 68.5-68.2 (-CH_2-CH_2-O-*C*H_2-COO-), 65.1/64.4 (-*C*H_2-CH_2-$(CH_2)_{10}$-CH_2-CH_2-COO-), 63.7/63.2 (-CH_2-*C*H_2-O-CH_2-COO-), 34.4/34.2 (-CH_2-CH_2-$(CH_2)_{10}$-CH_2-*C*H_2-COO-), 24.9–29.6 ppm (-CH_2-*C*H_2-(*C*H_2)$_{10}$-*C*H_2-CH_2-COO-).

2.3. Characterization of thermal and crystalline properties of PEG-poly(PDL-*co*-DO) block copolymers

Thermogravimetric analysis (TGA) measurements were performed with a TA Instruments Q500 Thermogravimetric Analyzer with High Resolution Mode, from room temperature to 600 °C at a heating rate of 10 °C/min in a nitrogen atmosphere. Differential scanning calorimetry (DSC) analysis was carried out using a TA Instruments Q2000 MDSC equipped with a refrigerated cooling system (RCS). The temperature scale was calibrated with high-purity standards. DSC scans were performed in the temperature range from −90 to 150 °C. Wide-angle X-ray diffraction measurements (WAXS) were carried out at room temperature with a PANalytical X'Pert PRO diffractometer equipped with an XCelerator detector. CuK radiation (λ = 0.15418 nm) was used as X-ray source. The degree of crystallinity (X_c) was evaluated as the ratio of the crystalline peak areas to the total area under the scattering curve. The amorphous and crystalline contributions were calculated by a fitting method using the WinFit program.

2.4. Nanoparticle preparation

PEG-poly(PDL-*co*-DO) NPs were fabricated using an emulsion-evaporation technique. PEG-poly(PDL-*co*-DO) block copolymer (25 mg) was dissolved in 0.5 ml dichloromethane (DCM) at room temperature. The organic phase was then added dropwise to 5 ml of DI water under a strong vortex and the resultant mixture was sonicated for three cycles of 10 s intervals followed by dilution in 15 ml of DI water. The final mixture was concentrated using a rotary evaporator, transferred to Amicon Ultra-15 100 kDa centrifugal filter unit, and then centrifuged at 4,000 g at 43°C for 40 min. The NPs were thrice washed with 10 ml DI water and centrifuged for 40 min. The washed NPs were immediately used, or snap-frozen in aliquots at −80 °C until use. Three groups of NPs were prepared using this method from

three PEG-poly(PDL-*co*-DO) copolymers with different compositions. Drug-loaded PEG-poly(PDL-*co*-DO) NPs were prepared similarly with addition of a drug encapsulant to the DCM organic phase prior to vortex. Fluorescent NPs were prepared with the addition of 0.05 mg of DiI and radiosensitizer NPs were prepared by adding 0.5 mg of VE822. Fluorescent NPs prepared from non-PEGylated poly(PDL-co-DO) polymer were prepared in the same method described above except the aqueous phase consisted of 2 wt% poly(vinyl alcohol) (Sigma-Aldrich Chemical) solution.

2.5. *In vitro* nanoparticle characterization

Size and zeta potential measurements—NPs were suspended in DI water (0.05 mg/ml) and the hydrodynamic sizes (Z-average diameters) of the particles (n=5) were analyzed by dynamic light scattering using a Malvern Nano-ZS (Malvern Instruments, UK). The same instrument was also used to measure the zeta potential of NPs (n=5).

TEM imaging—The morphologies of PEG-poly(PDL-*co*-DO) NPs were analyzed using a Tecnai T12 TEM microscope (FEI, Hillsboro, OR). NP solutions (0.05 mg ml^{-1}, 10 μl) were placed on clean and hydrophilized CF400-CU TEM grids (Electron Microscopy Sciences, Hatfield, PA, USA). The grids were stained with a 0.2% uranyl acetate solution for 15 s, washed three times in DI water, and then mounted for observation of NP images under the TEM microscope.

Hydrolytic degradation of PEG-poly(PDL-co-DO) nanoparticles—Blank PEG-poly(PDL-*co*-DO) NPs were suspended in 1x PBS at 37 °C on a rotary shaker set at 100 rpm for up to 28 d. At predetermined time intervals, a small fraction of the NP solution was removed and centrifuged to isolate NPs. The sediment formed after centrifugation was lyophilized and analyzed by gel permeation chromatography (GPC) using polystyrene standards to quantify the molecular weights of the degraded PEG-poly(PDL-*co*-DO) copolymer.

Particle stability in aCSF—Particle stability, quantified by variations of size and surface charge over time, was evaluated by a Malvern Nano-ZS in artificial cerebrospinal fluid (aCSF; Harvard Apparatus, Holliston, MA) at 37 °C for 28 d.

Drug loading in particles—VE822-loading in PEG-poly(PDL-co-DO) NP formulations was determined using a Shimadzu HPLC System (SpectraLab Scientific, Markham, ON, Canada) with ZORBAX Extend C18 analytical column (Agilent). Briefly, 1 mL NP solution at a concentration of 1 mg mL^{-1} was diluted 10-fold in Acetonitrile and filtered with a 10 kDA centrifugal filter unit (Amicon). The concentration of VE822 in these samples was quantified using the high-performance liquid chromatography (HPLC) apparatus (Agilent LCMS Q ESMS 6120B) equipped with an Eclipse Plus C18 (4.6 × 50 mm, 1.8 μm, 600 bar) column. The eluent, acetonitrile/diH_2O 60/40 (v/v) containing 0.1% trifluoroacetic acid (TFA), was set at a flow rate of 1 mL min^{-1} and the detector set at 309 nm. Standard curves were established using known drug concentrations processed (diluted and filtered) identically to the experimental samples. These curves were then used to determine the corresponding concentrations of VE822 in the experimental samples.

Drug release from particles—The release of VE822 from PEG-poly(PDL-*co*-DO) NPs was measured for up to 28 d after fabrication in sink conditions of the release medium. VE822-loaded NPs in 1x PBS with a surfactant, 0.5% Tween 80, were placed at 37 °C on a rotary shaker set at 100 rpm. At predetermined time points, an aliquot of the NP suspension was withdrawn and filtered. The filtrate was then analyzed by a Shimadzu HPLC System by the same method described above to determine the quantity of released radiosensitizer. The withdrawn NP solution was replaced by a same volume of the fresh buffer medium for further release study. Burst release was defined as percentage of initial loading released during the first 24 h. As a quantitative measure of sustained release *in vitro*, we defined the sustained phase of release as the period from 14 to 28 d of continuous incubation. We fit a linear regression model to the data to determine the rate of drug release during this period.

Western Blot—RG2 cells cultured under sterile conditions were treated with 750 nM of VE822-loaded PEG-poly(PDL-*co*-DO) NPs or free VE822. The cells without treatment were used as control. After treatment for 24 h, the cells were irradiated with 5 Gy using an XRAD 320 Cabinet X-ray irradiator (Precision Xray, CT, USA). Cells were harvested 60 min after radiation and prepared for Western Blot analysis using mouse monoclonal anti-Chk1 (2G1D5, Cell Signaling), rabbit monoclonal anti-pChk1 (SER345) (133D3, Cell Signaling), and Vinculin (Santa Cruz Biotechnology). as a loading control. This protocol was repeated for non-irradiated RG2 cells treated with 750 nM of VE822-loaded PEG-poly(PDL-*co*-DO) or free VE822 (Fig. S3). pChk1 protein levels of irradiated RG2 cells as depicted in Figure 3 were measured by normalizing to Vinculin and total Chk1 levels (Fig. S4).

2.6. *In vivo* nanoparticle characterization

All animal procedures were performed in accordance with the guidelines and policies of the Yale Animal Resource Center (YARC) and approved by the Institutional Animal Care and Use Committee (IACUC) per protocol # 2015-20060. Male Fischer 344 rats (Charles River Laboratories, 200–220 g) were used. Surgical procedures were performed with standard sterile surgical techniques.

Convection enhanced delivery—All animals were anaesthetized using a mixture of ketamine (75 mg kg^{-1}) and xylazine (5 mg kg^{1}) injected intraperitoneally. Rats' heads were then shaved and placed on a stereotaxic frame for immobilization. After sterilization of the scalp with betadine and alcohol, a midline scalp incision was made to expose the coronal and sagittal sutures. A burr hole was then drilled 3 mm lateral to the sagittal suture and 0.5 mm anterior to the bregma. A 50 μl Hamilton syringe with polyamide-tipped tubing was loaded with 20 μl of NP solution at 50 mg ml^{-1} and inserted into the burr hole. After 7 min of equilibration, a micro-infusion pump (World Precision Instruments, Sarasota, FL, USA) was used to infuse the NP solution at a rate of 0.667 μl min^{-1}. After complete infusion, the syringe was left in place for 7 min prior to removal. Bone wax was used to fill the burr hole and the skin was stapled and cleaned. Animals were placed in a heated cage until full recovery. CED in tumor-bearing rats was conducted following the same procedure as for healthy rats with delivery through the reopened burr hole used for tumor implantation

Orthotopic tumor implantation—Orthotopic RG2 tumors were inoculated as previously described. Briefly, 3 μl containing 2.5×10^5 RG2 cells suspended in PBS were administered over 3 min using the same procedure and coordinates as CED. Given the well-characterized, robust growth of RG2 orthotopic tumors in rats which others have been previously described [28–30] as well as our own experience that this infusion protocol reproducibly results in death approximately 15 days after inoculation [31, 32], tumors were grown for 4 d before beginning treatment to allow for a full 5-day course of radiation treatment after CED.

Volume of distribution—Volume of distribution was measured as previously described [20]. Briefly, rat brains were harvested at 4 h and 24 h after infusion of DiI dye-loaded NPs and flash frozen. Brains were sliced in 50 μm slices using a Leica Cryostat CM3000 (Leica, Germany). Slides were imaged using a Zeiss Lumar V12 stereoscope (Carl Zeiss AG, Germany). Volume of distribution was quantified using a MATLAB code setting a threshold with Otsu's method [33].

Intracranial drug retention—To measure intracranial radiosensitizer retention, 20 μl of radiosensitizer-loaded NPs, free radiosensitizer, blank NPs, or 1x PBS was delivered into the right caudate via CED as described above. Brains were harvested at predetermined time points after injection (0, 0.2, 0.5, 1, 3, or 7 d) and divided into left and right hemispheres. Each hemisphere was separately processed using ACN and centrifugation to extract hydrophobic compounds. Filtrate was analyzed for VE822 quantity using Agilent LCMS 6120B (Agilent Technologies, Santa Clara, CA) by comparison against a standard curve.

Radiotherapy and survival endpoints—Animals were inoculated with tumors exactly as described above. After tumor growth for 4 d, animals were randomized into two treatment groups: animals receiving radiation therapy and animals not receiving radiation therapy. Animals in each treatment group were then randomized into 4 sub-groups receiving either free radiosensitizer, radiosensitizer-loaded NPs, blank NPs, or 1x PBS. All 8 sub-groups had 8 total animals per treatment. Starting at 48 h after drug delivery as previously described, animals receiving radiation therapy were irradiated for 3 Gy per day for 5 consecutive days with treatments spaced 24 h apart [34]. Prior to receiving radiation, animals were anesthetized with a mixture of ketamine (75 mg kg^{-1}) and xylazine (5 mg kg^{1}), injected intraperitoneally. Animals were placed in a plexiglass holder with molded lead shielding to collinate the beam and allow for selective cranial irradiation in a XRAD 320 Cabinet X-ray irradiator (Precision Xray, CT, USA). The health status of all animals was monitored daily. Euthanization occurred after either a 15% or greater loss in body weight or when it was humanely necessary due to the presence of clinical symptoms from tumor progression. Median overall survival (MOS) was calculated by plotting Kaplan-Meier curves and comparing survival curves by the log-rank test

2.7. Data and graphical analysis

GraphPad Prism 7.01 was utilized for all graphing and data analysis. Statistical significance when comparing two groups was assessed by two-tailed Student unpaired t-test unless otherwise noted. Time-to-event analysis was analyzed by plotting Kaplan-Meier curves and survival curves were compared by the log-rank test. Significance is represented on plots as

*<0.05, **<0.01, ***<0.005, ****<0.001. Error bars represent standard deviations. ImageJ and Matlab were used for all image analyses. Differences in survival curves were determined by log-rank test.

3. Results

3.1. Synthesis and properties of PEG-poly(PDL-*co*-DO) block copolymers

PEG-poly(PDL-*co*-DO) diblock copolymers were synthesized via ring-opening copolymerization of ω–pentadecalactone (PDL) with *p*-dioxanone (DO) using *Candida antarctica* lipase B (CALB) as the catalyst and poly(ethylene glycol) methyl ether (MeO-PEG2K-OH) as the initiator (Scheme 1). The composition of the copolymers was controlled by adjusting the substrate ratio in the feeds (Table 1). It is notable that, due to thermodynamic limitations, the DO monomer in the feeds was not completely converted and incorporated into the polymer products [35, 36]. Consequently, the PDL/DO unit molar ratio of the copolymers is higher than the PDL/DO monomer molar ratio in their corresponding feeds. To ensure high colloidal stability of the copolymer micelles in aqueous medium, all synthesized polymers contain 36–40 wt% PEG. The molecular weights of the polymers were measured by gel permeation chromatography (GPC) using polystyrene standards, and their molecular structures were analyzed by nuclear magnetic resonance (NMR) spectroscopy. The PEG-poly(PDL-*co*-DO) copolymers possessed molecular weights (M_w) between 12,000 and 15,000 Da and polydispersity between 1.7 and 1.8. The proton and carbon-13 NMR spectra of the block copolymers are essentially identical to those of poly(PDL-*co*-DO) copolyesters [20] except that the former polymers exhibit an additional proton resonance at 3.65 ppm and a carbon-13 resonance at 70.55 ppm attributable to the ethylene oxide units (–CH_2–CH_2–O–) in the polymer chains. The polymer compositions (including PDL/DO unit ratio and PEG content) were calculated from the proton NMR spectra of the copolymers. The initiation of the PDL/DO copolymerization by MeO-PEG-OH dictates that the formed PEG-poly(PDL-*co*-DO) chains predominantly consist of diblock copolymer chains (Scheme 1).

The synthesized PEG-poly(PDL-*co*-DO) copolymers are thermally stable up to 200 °C under nitrogen gas with a temperature of maximum degradation rate (T_{max}) around 400 °C. PEG-poly(PDL-*co*-DO) copolymers are semicrystalline at room temperature and are characterized by two distinct crystalline phases: (i) a low melting temperature phase (melting temperature around 48 °C) attributed to the PEG fraction and consistent with the PEG amount in the different copolymers; (ii) a high melting temperature phase, attributed to the poly(PDL-*co*-DO) crystals. Copolymers with high amount of PDO tend to melt at higher temperature compared to those with lower PDO content (melting temperatures ranging from 75 °C to 82 °C), The analyzed copolymers had a total degree of crystallinity ranging from 51 to 55%. Detailed solid state characterizations of the PEG-poly(PDL-*co*-DO) block copolymers are provided in the Supporting Information document (Table S1, Fig. S1–2).

3.2. Characterization of blank and radiosensitizer-loaded PEG-poly(PDL-*co*-DO) nanoparticles

PEG-poly(PDL-*co*-DO) copolymers were formulated into NPs that fit the criteria we previously described as “brain penetrating” [21, 23]. These blank NPs possess a mean hydrodynamic diameter ranging from 60–100 nm (Fig. 1a–c), spherical morphology (Fig. 1d–f), did not aggregate after incubation in artificial cerebrospinal fluid at 37 °C for up to 28 d (Fig. 1g), and had a negative surface charge (Table 2). The polydispersity index (PDI) of all NP samples was below 0.2 indicating a monodisperse population. The particle yield of all three copolymers was around 60% (Table 2), which is comparable to NPs formulated using similar polymers and the emulsion solvent evaporation technique [21, 24].

Additionally, the hydrolytic degradation of blank PEG-poly(PDL-*co*-DO) NPs was measured by the decrease in NP size and molecular weight over 28 d of incubation in artificial cerebrospinal fluid at 37 °C. Over this period, the average hydrodynamic diameter of the three NP samples decreased by ~15 nm (Fig. 1g) and the weight-average molecular weight (M_w) of the copolymers decreased by approximately 1,500 Da (Fig. 1h).

Encapsulation of VE822 within PEG-poly(PDL-*co*-DO) NPs did not significantly alter NP size, surface charge, or yield when compared to the blank NPs (Table 2). Of note, the drug encapsulation efficiency increases as the PDL to DO unit ratio in the copolymer increases.

3.3. *In vitro* drug release and functional activity profile of radiosensitizer-loaded PEG-poly(PDL-*co*-DO) nanoparticles

PEG-poly(PDL-*co*-DO) NPs exhibited biphasic release of encapsulated VE822 that included a period of rapid drug release within 24 h after encapsulation, the burst phase, during which 29, 17 and 9.1% of encapsulated VE822 were released by the NPs formulated from P56D44, P65D35 and P71D29, respectively (Table 3). During the sustained release phase—which we define as occurring from day 14 of incubation to day 28—0.8, 0.6 and 0.6% of loaded VE822 was released per day (Table 3) resulting in a cumulative total release of 67, 55 and 43% of encapsulated drug after 28 days for NPs formulated from P56D44, P65D35 and P71D29, respectively (Fig. 2).

The functional activity of PEG-poly(PDL-*co*-DO) NPs was evaluated by examining the biochemical effects of free radiosensitizer and radiosensitizer-loaded NPs on a known ionizing radiation-induced phosphorylation target, Chk1. ATR-dependent phosphorylation of Serine 345 (S345) on Chk1 leading to homologous recombination (HR) in response to ionizing radiation has been previously described and VE822 has also been shown to prevent this process [27, 37]. VE822-loaded NPs prepared from P56D44 and P65D35 copolymer inhibited ionizing radiation-induced phosphorylation of Chk1 in RG2 glioma cells to comparable levels observed with free VE822 after 24 h of pre-treatment and radiation therapy while VE822-loaded NPs prepared from P71D29 copolymer suppressed pChk1 below cells receiving no treatment but slightly less than free VE822 (Fig. 3).

3.4. *In vivo* volume of distribution and retention of PEG-poly(PDL-*co*-DO) nanoparticles after CED

The volume of distribution (V_d) achieved after CED of 20 μl (20 mm^3) of P56D44, P65D35, or P71D29 copolymer NPs after 24 h was 21, 46 and 59 mm^3, respectively (Fig. 4a–c). With a volume of injection (V_i) of 20 μl, these values correspond to V_d/V_i ratios of 1.1, 2.3 and 3.0 for NPs formulated from P56D44, P65D35 and P71D29, respectively. While the V_d/V_i ratio correlated with NP diameter, interestingly, larger particles exhibited better sustained penetration. From 4 to 24 h after infusion, V_d decreased for P56D44, P65D35 and P71D29 NPs, with the latter decreasing the least (Fig. 4d). After 24 h, the V_d of P71D29 NPs was significantly greater than the V_d of P56D44 NPs ($p < 0.01$). The V_d achieved after CED of NPs formulated from non-PEGylated poly(PDL-co-DO) copolymer was 1 mm^3 after 4 h and 0 mm^3 after 24 h. While not included in this study, previous data suggests that similarly sized NPs with PEG coating penetrate to an initial extent immediately after infusion (45 mm^3) [23, 31]. We have included this predicted data point on Fig. 4d for comparison.

To evaluate the influence of CED of NPs on duration of VE822 levels in the brain, VE822 concentration in the right hemisphere was measured for animals that received infusions of either free VE822 or VE822-loaded PEG-poly(PDL-*co*-DO) NPs (Fig. 5). For CED of the free drug, retention was short-lived: the percent retention was well-represented by first-order (exponential) decay with a half-life of 9 h, resulting in negligible amounts detectable after 48 h ($R^2 = 0.99$) [19] After CED of VE822-loaded P56D44 NPs, intracranial VE822 levels followed a similar pattern as free VE822 with a half-life of 12 h and 15% of the drug remaining 24 h post injection. Clearance from intracranial tissue of VE822 delivered in P65D35 and P71D29 NPs occurred more slowly with half-lives of approximately 2 d and 5 d respectively, which are also well represented by an exponential decay model ($R^2 = 0.99$). After 1 week, P71D29 NPs exhibited the greatest retention of VE822 with 43% of injected drug detected within the right hemisphere (Fig. 5). VE822 was not detected in the left hemisphere for any group at any time point.

3.5. Enhanced therapeutic benefits of VE822-loaded PEG-poly(PDL-*co*-DO) nanoparticles in a rat intracranial xenograft model

The therapeutic efficacy of VE822-loaded PEG-poly(PDL-*co*-DO) NPs was tested by administrating the NPs via CED to rats bearing RG2-derived gliomas followed by fractionated radiation therapy (FRT) (Fig. 6a). The P71D29 NP formulation was chosen for this study due to its superior volume of distribution after 24 h (Fig. 4c), prolonged release (Fig. 2), and enhanced retention of the drug within the brain tissue when compared to the NPs formulated from P56D44 and P65D35 (Fig. 5). We used the RG2 glioma model because inoculation of RG2 cells into the brains of syngeneic Fischer 344 rats has been well-established as a reproducible intracranial tumor model with predicted MOS of 14 d and infiltrative growth [38]. As described above, rats were separated into 2 groups, one group receiving FRT and another not receiving FRT. These groups were further divided into 4 sub-groups to identify if the VE822-loaded NPs conferred a unique survival advantage compared to unloaded NPs and free VE822. All sub-groups of rats not receiving FRT had MOS of 15 d, and there was no significant difference in survival between the rats receiving VE822-loaded NPs and any other sub-group using the log-rank test (Fig. 6b, d). However, in the

group receiving FRT, the rats treated with the VE822-loaded NPs lived significantly longer than all other subgroups as defined by the log-rank test ($p < 0.001$). The MOS of this sub-group, 23 d, is 21% longer compared to rats receiving FRT in the no treatment, blank NPs and free VE822 sub-groups—19 d for all sub-groups (Fig. 6b, d). The survival advantage conferred by the VE822-loaded poly(PDL-*co*-DO) NPs was also significantly greater in the FRT group compared to the non-FRT group ($p < 0.001$, Fig. 6c). Importantly, free VE822 did not provide a statistically significant survival advantage in rats receiving FRT. We note that all control animals (receiving no treatment) died of histologically confirmed tumors with MOS matching previous reports of the RG2 model [34, 39, 40].

4. Discussion

In this report, we demonstrate that PEG-poly(PDL-*co*-DO) copolymers can be formed into small nanoparticles which allow for prolonged release of encapsulated agents after administration by CED. Additionally, radiosensitizer-loaded PEG-poly(PDL-*co*-DO) NPs confer a significant survival advantage to tumor-inoculated rats receiving FRT. These results provide evidence for the potential of PEG-poly(PDL-*co*-DO) NPs in clinical applications requiring sustained drug release. One main advantage of these NPs is that their properties can be readily altered by adjusting the comonomer unit ratio in PEG-poly(PDL-*co*-DO) chains. Specifically, we determined how NP size, encapsulant release rate, intracranial retention and volume of distribution can be tuned by varying the ratio of PDL to DO repeat units in the copolymer. Previously, poly(PDL-*co*-DO) copolyesters were successfully utilized to fabricate NPs that were non-toxic and exhibited controlled and continuous release of encapsulated drug over 28 days [19]. Moreover, poly(PDL-*co*-DO) NP degradation rate was found to vary over a wide range depending on the copolymer composition, suggesting that drug release rate could also be altered [24]. The prolonged and potentially tunable release properties of poly(PDL-*co*-DO) NPs are promising for intracranial drug delivery. Nevertheless, these NPs had prohibitively large sizes (> 250 nm) to be suitable for applications in the brain. We hypothesized that conjugation of PEG to poly(PDL-*co*-DO) chains would allow fabrication of smaller NPs and facilitate the use of the resultant PEG-poly(PDL-*co*-DO) copolymers in the setting of the brain.

It has long been known that block copolymers of PEG with degradable polyesters can be used to produce NPs with surface PEG groups that enhance NP biodistribution and pharmacokinetics [41]. PEGylation has been investigated in the context of prolonging intracranial retention following local delivery [42, 43] and in a recent study examining PEGylated squalenoyl-gemcitabine NPs for the treatment of glioblastoma, PEGylated NPs distributed more uniformly and aggregated less after CED at the site of infusion when compared to their non-PEGylated counterparts [31]. Therefore, we synthesized and evaluated three PEG-poly(PDL-*co*-DO) diblock copolymers with different PDL/DO unit ratios: P56D44, P65D35 and P71D29.

All PEG-poly(PDL-*co*-DO) NP formulations obtained were monodisperse (PDI < 0.2) and NP characteristics did not vary significantly when loaded with dye or VE822 (Table 2). The three different copolymer compositions yielded varying encapsulation efficiencies ranging from 25–42% with increasing PDL content associated with greater encapsulation. The

encapsulation efficiency of VE822 is likely correlated with the PDL content in the copolymers due to hydrophobic interactions between the highly hydrophobic PDL and VE822 within the emulsion during NP fabrication. These results are comparable with the encapsulation efficiencies achieved by another recent study that encapsulated VE822 within a polylactic acid-PEG (PLA-PEG) NP system [34].

Hydrophobic interaction between PDL monomer units and VE822 likely contributed to the substantially different burst release of loaded-VE822 within the first 24 h for each PEG-poly(PDL-*co*-DO) copolymer formulation. The copolymer with the greatest PDL content, P71D29, formed NPs with the smallest burst release of 9.1% within the first 24 h whereas P56D44 NPs yielded a burst release of 29% over this same time period. The rapid release of the drug during the first 24 h likely resulted from the release from drug molecules associated with the surface of the NPs, as well as the degree of initial water penetration into the polymer matrix [44, 45]. Therefore, we hypothesize that higher PDL content slows the release of drug due to hydrophobic interaction between the copolymer and the drug and limited aqueous infiltration to the polymer matrix. The limited drug burst release of the P71D29 and P65D35 NPs is a significant advantage for PEG-poly(PDL-*co*-DO) NPs over other polymeric nanocarrier systems such as PLGA, which often release greater than half of encapsulated drug within initial 24 h [44–48]. It was reported that even those PLGA systems designed for sustained release of small-molecule hydrophobic radiosensitizers (e.g., VE822) released 45–70% of encapsulant within the first 24 h [49, 50]. Despite the low levels of burst release, we found that VE822-loaded NPs were sufficient for radiosensitization. When RG2 cells were treated with VE822-loaded NPs for 24 h, HR was blocked *in vitro* at levels comparable to those exhibited by the free drug (Fig. 3). Particularly, the P56D44 and P65D35 NP samples appeared to have the greatest radiosensitizing effect which is consistent with their greater VE822 release in the first 24 h compared to P79D21 NPs.

An additional advantage of decreased burst release is sustained release of encapsulated drug for weeks after the initial exposure to water (Fig. 2). As previously reported, poly(PDL-*co*-DO) copolyesters are copolymers of an isodimorphic system [24]. Thus, the sustained release capabilities of NPs formulated from this copolymer are likely due to slow polymer chain hydrolysis associated with less-accessible crystalline phases of the copolymers. The rate of polymer degradation hydrolytic degradation was measured via GPC and it was observed that all PEG-poly(PDL-*co*-DO) NP samples degraded by ~1,500 Da over 28 days (which represents 11% total molecular weight degradation, Fig. 1h). In comparison, previous studies reported that PLGA degrades much more rapidly with 90+% weight average molecular weight decrease after 10 days, contributing to greater burst release rates and less sustained release capabilities beyond the period of 2 weeks [51–53]; A recent study encapsulating similar small-molecule radiosensitizers to VE822 within PLGA NP observed 90% release of encapsulated drug within just 3 days [50].

In this study, we demonstrate the inability of non-PEGylated poly(PDL-*co*-DO) NPs to distribute within the brain ($V_d/V_i < 0.5$). This is likely due to their much larger diameters (~300 nm) compared to PEGylated poly(PDL-*co*-DO), inhibiting penetration through the brain interstitium and lack of hydrophilic PEG coating, which might result in significant aggregation at the site of infusion. PEG-poly(PDL-*co*-DO) NPs were able to penetrate the

brain interstitium during CED. The V_d/V_i ratios of the P56D44, P65D35 and P71D29 NPs at 24 h after CED were 1.1, 2.3 and 3.0, respectively. Although lower than the theoretical limit of $V_d/V_i = 5$ (which can be observed for small molecules capable of freely distributing with fluid through the brain extracellular space) [54], these values are comparable to previous values achieved after CED infusion of NPs [21, 31]. Our results also suggest that NP diameter may play a role in sustained penetration in the brain as the largest particles, P71D29 (106 nm) retained a V_d of 50 mm^3 24 h after CED while the smallest particles, P56D44 have good early penetration (4 h) but V_d is substantially lower at 24 h. These findings suggest that distribution and retention within the brain is influenced by NP diameter and we believe this is an important point to study more completely in the future. Additionally, diffusion of drug released from NPs, which is further affected by rate of release of drug, may play a role in the differing V_d observed between the three polymers. Although we do not currently have the technical capability to simultaneously image NPs and released drug, this topic clearly deserves further study. Because tumors are very small at the time of CED delivery, we do not expect relative levels of infused VE822 (V_d) to vary significantly in a tumor-bearing rat brain. Also, previous studies have shown that the presence of a tumor modifies the pattern of distribution, it does not significantly modify the particle volume of distribution [31, 32]. For similar reasons, we do not expect drug retention to vary significantly between non-tumor and tumor-bearing rat brains. However, our understanding of an intracranial tumor's effects on drug retention, specifically drug-releasing NPs after CED, is limited and we have yet to optimize the preferential distribution of CED-delivered radiosensitizer to tissue containing tumor cells.

Our *in vitro* and *in vivo* experiments revealed that the nanoparticles formed from three PEG-poly(PDL-*co*-DO) copolymers with different compositions possessed a wide range of release, distribution and retention characteristics. Among these three copolymers, P71D29 was selected to test therapeutic efficacy due to its superior distribution and retention profiles, which are key to tumor treatment with FRT. Prolonged drug retention is especially beneficial for treatment because methods of local drug delivery into the brain (e.g., CED) are invasive. Therefore, it is important to maintain clinical efficacy with a minimal number of surgical procedures. To ensure coverage of a disperse, infiltrative tumor, it is also essential to achieve a large volume of distribution. We believe that the significantly improved survival of the rats treated with the VE822-loaded NPs vs free VE822 is attributable to (i) the prolonged release and retention of the drug with half-life of ~ 5 days (half-life of free VE822 is ~ 10 h), (ii) capability of the NP formulation to maintain intracranial drug levels above the previously reported IC50 of VE822 (0.125 μM) over one week, and (iii) the sufficient drug distribution [34]. We note that the VE822-loaded NPs are unable to completely cure tumor-bearing rats, possibly due to a suboptimal FRT schedule after NP infusion or incomplete coverage of tumor mass which has previously been described in the context of polymeric NPs [32]. Although we are currently unable to quantify the changing intracellular concentration of VE822 *in vivo* over time, this will be important in future work in order to identify the optimal FRT dosing strategy. While further research is necessary to maximize the clinical efficacy of PEG-poly(PDL-*co*-DO) NP formulations in this multimodality treatment, our results clearly demonstrate that maintaining sufficient intracranial levels of radiosensitizer throughout FRT treatment is key to inhibiting DNA repair and prolonging survival.

Although PEG-poly(PDL-*co*-DO) NPs were utilized in this study to deliver small molecule radiosensitizers, this nanocarrier platform can be tailored for treatment of a host of CNS diseases requiring local administration of therapeutic agents. In the current work, a larger volume of distribution is desired due to the infiltrative nature of RG2 glioma tumor models and because VE822 ATR inhibition is not cytotoxic to non-tumoral cells after RT [27]. The PDL-rich P71D29 NPs were efficient for delivery of agents requiring sustained intracranial presence. Alternatively, use of PEG-poly(PDL-*co*-DO) NPs with a low PDL content can yield decreased intracranial drug retention if shorter exposure of therapeutic agents is desired. Moreover, treatments targeting variable volumes of localized cerebral dysfunction (e.g., stroke) could utilize such NP carriers for focused delivery of encapsulated agents [55]. Importantly, we have shown that PEG-poly(PDL-*co*-DO) nanocarriers are capable of delivering encapsulated agent for therapeutic effect with sustained intracranial retention and widespread distribution, and that these properties can be modulated by altering the copolymer composition.

5. Conclusions

This study demonstrates the ability of PEG-poly(PDL-*co*-DO) nano-formulations to successfully deliver loaded therapeutic agent intracranially. We show that the conjugation of PEG allows for small nanoparticles and widespread drug distribution within the brain after infusion by CED while preserving the sustained release properties of poly(PDL-*co*-DO) copolymer. Administration of VE822-loaded PEG-poly(PDL-*co*-DO) NPs, compared to free VE822, in combination with FRT provided statistically significant survival benefits in animals bearing orthotopic RG2 tumors. Finally, PEG-poly(PDL-*co*-DO) NPs exhibited a wide range of composition-dependent drug release, distribution and retention characteristics. Altogether, these results indicate that PEG-poly(PDL-*co*-DO) copolymers have a great potential to be utilized as a versatile and long-acting NP release system for broad treatment of intracranial diseases.

Supplementary Material

Refer to Web version on PubMed Central for supplementary material.

Acknowledgments

The authors thank Marc Llaguno for his assistance acquiring TEM images and Dr. Terence Wu for his help with LC-MS. This work was supported by the National Institutes of Health (R01 CA149128 and F30 CA206386), the Musella Foundation, and a Yale Cancer Center Collaborative Co-Pilot Award. Christopher Jackson is an HHMI Medical Research Fellow. Alex Josowitz is an NSF Graduate Fellow.

References

1. Ferrari M. Cancer nanotechnology: opportunities and challenges. Nat Rev Cancer. 2005; 5(3):161–71. [PubMed: 15738981]
2. Gindy ME, Prud'homme RK. Multifunctional nanoparticles for imaging, delivery and targeting in cancer therapy. Expert Opin Drug Deliv. 2009; 6(8):865–78. [PubMed: 19637974]
3. Shi J, et al. Self-assembled targeted nanoparticles: evolution of technologies and bench to bedside translation. Acc Chem Res. 2011; 44(10):1123–34. [PubMed: 21692448]

4. Li SD, Huang L. Pharmacokinetics and biodistribution of nanoparticles. Mol Pharm. 2008; 5(4): 496–504. [PubMed: 18611037]
5. Phillips MA, Gran ML, Peppas NA. Targeted Nanodelivery of Drugs and Diagnostics. Nano Today. 2010; 5(2):143–159. [PubMed: 20543895]
6. Amoozgar Z, Yeo Y. Recent advances in stealth coating of nanoparticle drug delivery systems. Wiley Interdiscip Rev Nanomed Nanobiotechnol. 2012; 4(2):219–33. [PubMed: 22231928]
7. Deng Y, et al. The effect of hyperbranched polyglycerol coatings on drug delivery using degradable polymer nanoparticles. Biomaterials. 2014; 35(24):6595–602. [PubMed: 24816286]
8. Moghimi SM, Hunter AC, Murray JC. Long-circulating and target-specific nanoparticles: theory to practice. Pharmacol Rev. 2001; 53(2):283–318. [PubMed: 11356986]
9. Sethi K, Roy I. Organically modified titania nanoparticles for sustained drug release applications. J Colloid Interface Sci. 2015; 456:59–65. [PubMed: 26093234]
10. Panyam J, Labhasetwar V. Biodegradable nanoparticles for drug and gene delivery to cells and tissue. Adv Drug Deliv Rev. 2003; 55(3):329–47. [PubMed: 12628320]
11. Lin SY, et al. In vitro degradation and dissolution behaviours of microspheres prepared by three low molecular weight polyesters. J Microencapsul. 2000; 17(5):577–86. [PubMed: 11038117]
12. Saraiva C, et al. Nanoparticle-mediated brain drug delivery: Overcoming blood-brain barrier to treat neurodegenerative diseases. J Control Release. 2016; 235:34–47. [PubMed: 27208862]
13. Costantino L, Boraschi D, Eaton M. Challenges in the design of clinically useful brain-targeted drug nanocarriers. Curr Med Chem. 2014; 21(37):4227–46. [PubMed: 25039774]
14. Kreuter J. Drug delivery to the central nervous system by polymeric nanoparticles: what do we know? Adv Drug Deliv Rev. 2014; 71:2–14. [PubMed: 23981489]
15. Gao H, Pang Z, Jiang X. Targeted delivery of nano-therapeutics for major disorders of the central nervous system. Pharm Res. 2013; 30(10):2485–98. [PubMed: 23797465]
16. Saucier-Sawyer JK, et al. Systemic delivery of blood-brain barrier-targeted polymeric nanoparticles enhances delivery to brain tissue. J Drug Target. 2015; 23(7–8):736–49. [PubMed: 26453169]
17. Bobo RH, et al. Convection-enhanced delivery of macromolecules in the brain. Proc Natl Acad Sci U S A. 1994; 91(6):2076–80. [PubMed: 8134351]
18. Healy AT, Vogelbaum MA. Convection-enhanced drug delivery for gliomas. Surg Neurol Int. 2015; 6(Suppl 1):S59–67. [PubMed: 25722934]
19. Vecchio D, et al. Pharmacokinetics, pharmacodynamics and efficacy on pediatric tumors of the glioma radiosensitizer KU60019. Int J Cancer. 2015; 136(6):1445–57. [PubMed: 25091220]
20. Sawyer AJ, et al. Convection-enhanced delivery of camptothecin-loaded polymer nanoparticles for treatment of intracranial tumors. Drug Deliv Transl Res. 2011; 1(1):34–42. [PubMed: 21691426]
21. Zhou J, et al. Highly penetrative, drug-loaded nanocarriers improve treatment of glioblastoma. Proc Natl Acad Sci U S A. 2013; 110(29):11751–6. [PubMed: 23818631]
22. Nance EA, et al. A dense poly(ethylene glycol) coating improves penetration of large polymeric nanoparticles within brain tissue. Sci Transl Med. 2012; 4(149):149ra119.
23. Song E, et al. Surface chemistry governs cellular tropism of nanoparticles in the brain. Nat Commun. 2017; 8:15322. [PubMed: 28524852]
24. Liu J, et al. Biodegradation, biocompatibility, and drug delivery in poly(omega-pentadecalactone-co-p-dioxanone) copolyesters. Biomaterials. 2011; 32(27):6646–54. [PubMed: 21641030]
25. Jiang Z, et al. Lipase-catalyzed copolymerization of omega-pentadecalactone with p-dioxanone and characterization of copolymer thermal and crystalline properties. Biomacromolecules. 2007; 8(7):2262–9. [PubMed: 17550288]
26. King AR. Yale University Department of Biomedical Engineering. Yale University; 2016. Convection-enhanced delivery of radiosensitizer-loaded nanoparticles for the treatment of pediatric brainstem gliomas.
27. Fokas E, et al. Targeting ATR in vivo using the novel inhibitor VE-822 results in selective sensitization of pancreatic tumors to radiation. Cell Death Dis. 2012; 3:e441. [PubMed: 23222511]
28. Barth RF, Kaur B. Rat brain tumor models in experimental neuro-oncology: the C6, 9L, T9, RG2, F98, BT4C, RT-2 and CNS-1 gliomas. J Neurooncol. 2009; 94(3):299–312. [PubMed: 19381449]

29. Boult JK, et al. Investigating intracranial tumour growth patterns with multiparametric MRI incorporating Gd-DTPA and USPIO-enhanced imaging. NMR Biomed. 2016; 29(11):1608–1617. [PubMed: 27671990]
30. Krajewski S, Kiwit JC, Wechsler W. RG2 glioma growth in rat cerebellum after subdural implantation. J Neurosurg. 1986; 65(2):222–9. [PubMed: 2425062]
31. Gaudin A, et al. PEGylated squalenoyl-gemcitabine nanoparticles for the treatment of glioblastoma. Biomaterials. 2016; 105:136–44. [PubMed: 27521616]
32. Saucier-Sawyer JK, et al. Distribution of polymer nanoparticles by convection-enhanced delivery to brain tumors. J Control Release. 2016; 232:103–12. [PubMed: 27063424]
33. Chi DL, et al. Improved threshold selection for the determination of volume of distribution of nanoparticles administered by convection-enhanced delivery. Comput Med Imaging Graph. 2017; 62:34–40. [PubMed: 28927549]
34. King AR, et al. Local DNA Repair Inhibition for Sustained Radiosensitization of High-Grade Gliomas. Mol Cancer Ther. 2017; 16(8):1456–1469. [PubMed: 28566437]
35. Yang KK, Wang XL, Wang YZ. POLY(p-DIOXANONE) AND ITS COPOLYMERS. Journal of Macromolecular Science, Part C. 2002; 42(3):373–398.
36. Nishida H, et al. Equilibrium Polymerization Behavior of 1,4-Dioxan-2-one in Bulk. Macromolecules. 2000; 33(19):6982–6986.
37. Liu Q, et al. Chk1 is an essential kinase that is regulated by Atr and required for the G(2)/M DNA damage checkpoint. Genes Dev. 2000; 14(12):1448–59. [PubMed: 10859164]
38. Franken NA, et al. Clonogenic assay of cells in vitro. Nat Protoc. 2006; 1(5):2315–9. [PubMed: 17406473]
39. Brinker T, Lewis A. Rat Model of Malignant Brain Tumors: Implantation of Doxorubicin Using Drug Eluting Beads for Delivery. In: Hayat MA, editorTumors of the Central Nervous System, Volume 4: Brain Tumors (Part 2). Springer Netherlands; Dordrecht: 2012. 249–255.
40. Wahlberg LU, et al. Polymeric controlled-release amsacrine chemotherapy in an experimental glioma model. Acta Neurochir (Wien). 1996; 138(11):1323–9. discussion 1329–30. [PubMed: 8980737]
41. Gref R, et al. Biodegradable long-circulating polymeric nanospheres. Science. 1994; 263(5153): 1600–3. [PubMed: 8128245]
42. Nance E, et al. Brain-penetrating nanoparticles improve paclitaxel efficacy in malignant glioma following local administration. ACS Nano. 2014; 8(10):10655–64. [PubMed: 25259648]
43. Zhang C, et al. Convection enhanced delivery of cisplatin-loaded brain penetrating nanoparticles cures malignant glioma in rats. J Control Release. 2017
44. Makadia HK, Siegel SJ. Poly Lactic-co-Glycolic Acid (PLGA) as Biodegradable Controlled Drug Delivery Carrier. Polymers (Basel). 2011; 3(3):1377–1397. [PubMed: 22577513]
45. Allison SD. Analysis of initial burst in PLGA microparticles. Expert Opin Drug Deliv. 2008; 5(6): 615–28. [PubMed: 18532918]
46. Matsumoto J, et al. Preparation of nanoparticles consisted of poly(L-lactide)-poly(ethylene glycol)-poly(L-lactide) and their evaluation in vitro. Int J Pharm. 1999; 185(1):93–101. [PubMed: 10425369]
47. Wang Y, Li P, Kong L. Chitosan-modified PLGA nanoparticles with versatile surface for improved drug delivery. AAPS PharmSciTech. 2013; 14(2):585–92. [PubMed: 23463262]
48. Han FY, et al. Bioerodable PLGA-Based Microparticles for Producing Sustained-Release Drug Formulations and Strategies for Improving Drug Loading. Front Pharmacol. 2016; 7:185. [PubMed: 27445821]
49. Menon JU, et al. Polymeric nanoparticles for targeted radiosensitization of prostate cancer cells. J Biomed Mater Res A. 2015; 103(5):1632–9. [PubMed: 25088162]
50. Tian X, et al. Improving DNA double-strand repair inhibitor KU55933 therapeutic index in cancer radiotherapy using nanoparticle drug delivery. Nanoscale. 2015; 7(47):20211–9. [PubMed: 26575637]
51. Park TG. Degradation of poly(lactic-co-glycolic acid) microspheres: effect of copolymer composition. Biomaterials. 1995; 16(15):1123–30. [PubMed: 8562787]

52. Birnbaum DT, Brannon-Peppas L. Molecular weight distribution changes during degradation and release of PLGA nanoparticles containing epirubicin HCl. J Biomater Sci Polym Ed. 2003; 14(1): 87–102. [PubMed: 12635772]

53. Wang EC, et al. Nanoparticle formulations of histone deacetylase inhibitors for effective chemoradiotherapy in solid tumors. Biomaterials. 2015; 51:208–15. [PubMed: 25771011]

54. Nicholson C, Sykova E. Extracellular space structure revealed by diffusion analysis. Trends Neurosci. 1998; 21(5):207–15. [PubMed: 9610885]

55. Hardas SS, et al. Brain distribution and toxicological evaluation of a systemically delivered engineered nanoscale ceria. Toxicol Sci. 2010; 116(2):562–76. [PubMed: 20457660]

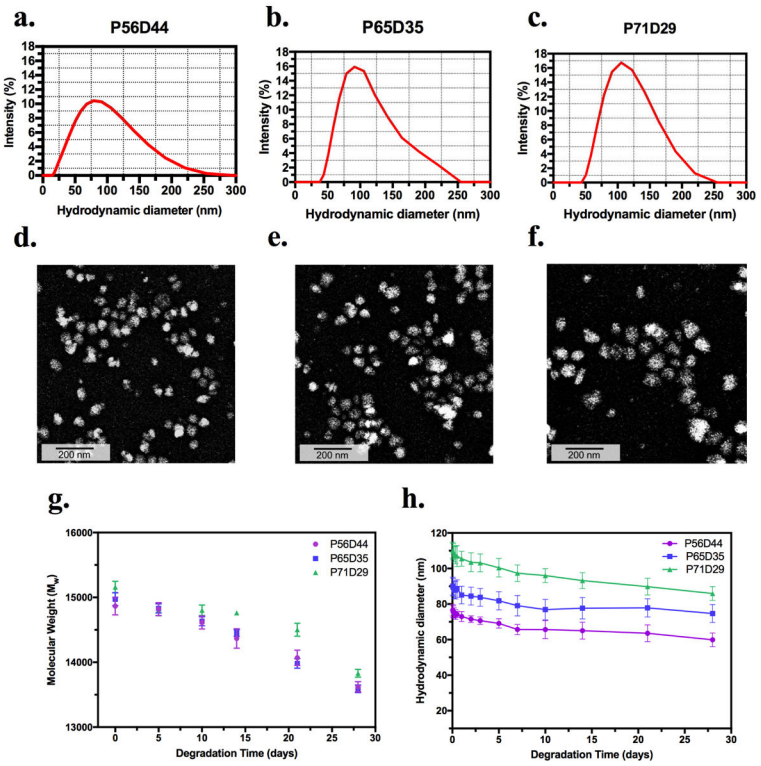

Figure 1. Nanoparticle characterization

Hydrodynamic diameter distributions and TEM images of P56D44 (a, d), P65D35 (b, e), and P71D29 (c, f) blank nanoparticles suspended in diH2O, and their size changes (g) in aCSF and molecular weight variations (h) in PBS at 37 °C as a function of time. Data in Fig. 1g and h is shown as mean ± SEM (n=5).

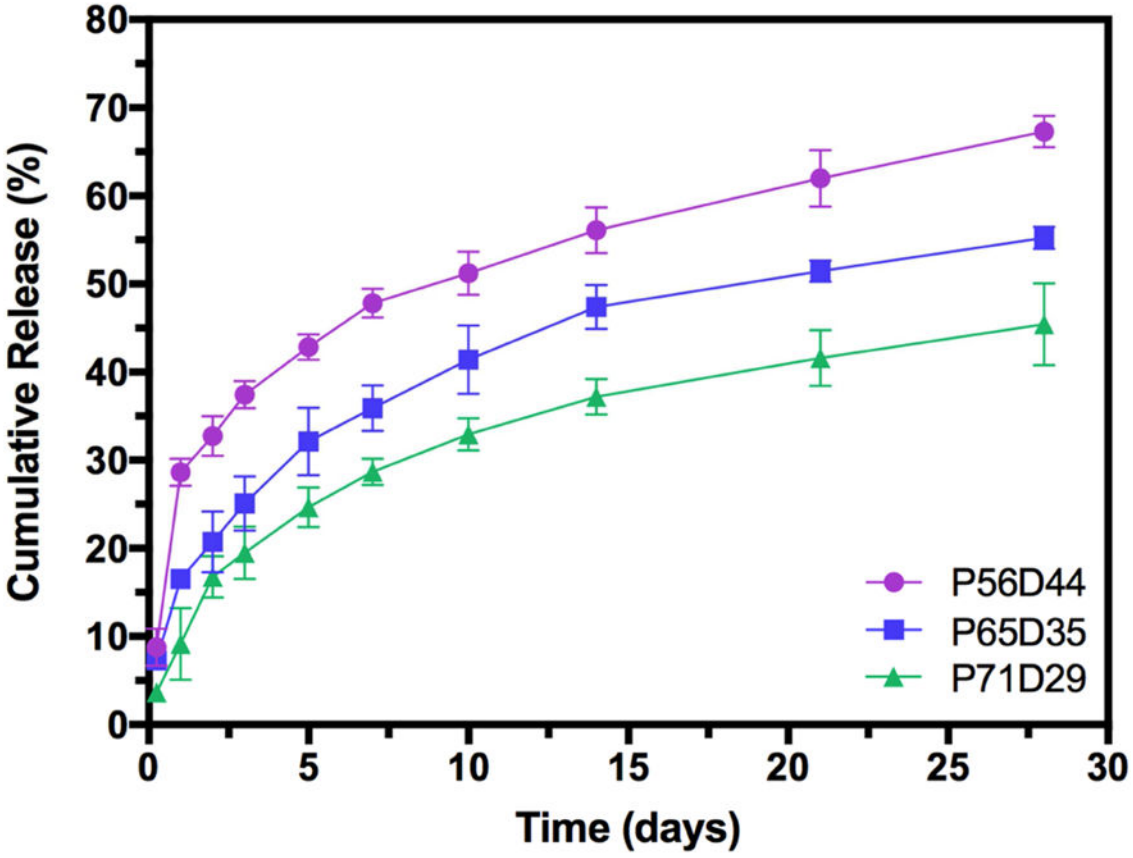

Figure 2. ***In vitro*** **drug release**

Release of encapsulated VE822 from P56D44, P65D35 and P71D29 nanoparticles at 37 °C in PBS with 0.5% Tween 80.

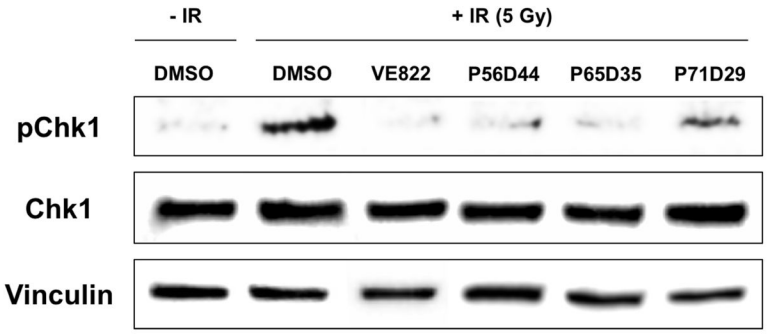

Figure 3. VE822-loaded nanoparticle protein regulation

Western blot of Phospho-Chk1 levels in radiated (right five columns), and non-radiated (left column) RG2 cells. Cells were treated for 24 h with no treatment (DMSO), VE822-loaded P56D44 nanoparticles (P56D44), VE822-loaded P65D35 nanoparticles (P65D35), VE822-loaded P71D29 nanoparticles (P71D29) or free VE822 (VE822). Vinculin is shown as a loading control.

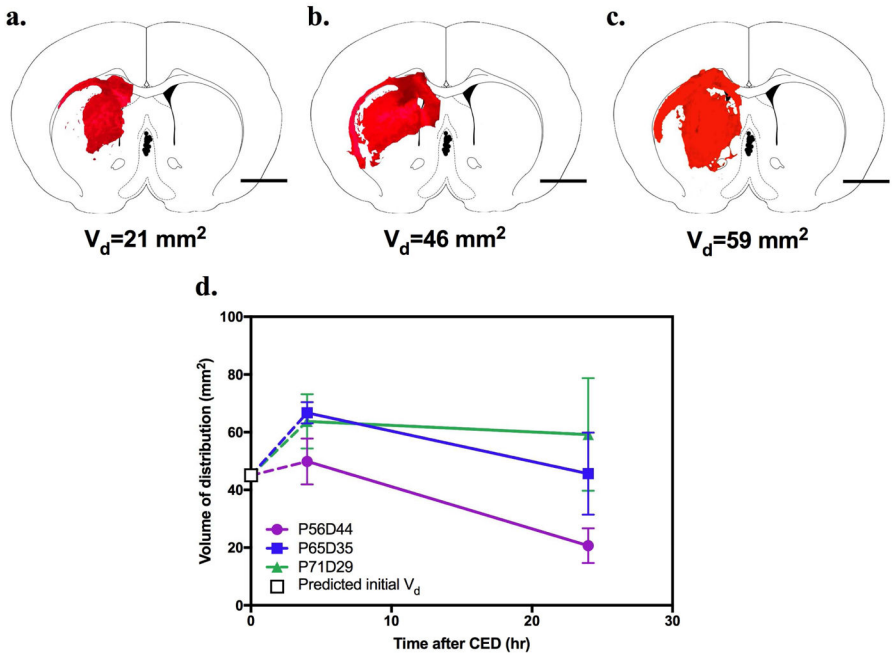

Figure 4. Nanoparticle volume of distribution

Visualized distribution of P56D44 (a), P65D35 (b) and P71D39 (c) nanoparticles loaded with DiI fluorescent dye 24 h after infusion. (d) *In vivo* comparison of DiI-loaded nanoparticle distribution in normal rat brain 4 h and 24 h following CED. Predicted initial V_d (white box at t=0) of 45 mm^3 is depicted with white box. Error bars represent the standard deviation of the mean volume of distribution for three separate animals, scale bar, 4 mm).

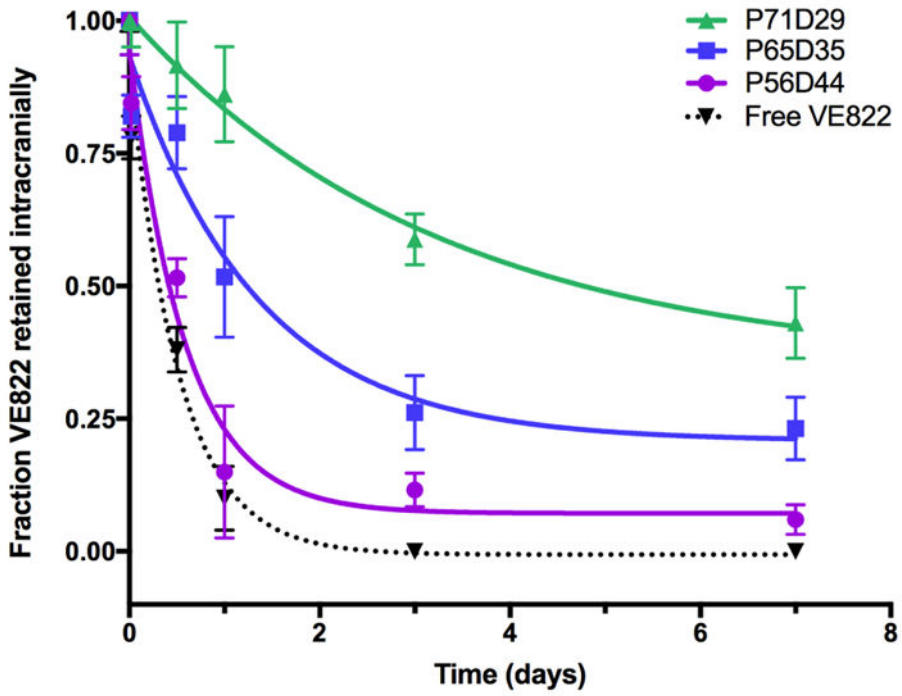

Figure 5. Intracranial nanoparticle retention

Fractional retention of VE822 in intracranial tissue following CED of free VE822, VE822-loaded P56D44, P65D35 or P71D29 nanoparticles. The data were analyzed using *ex vivo* standards of brains spiked with the drug. Saline solutions with an equivalent volume of DMSO (drug solvent) or an equivalent weight of blank NPs were measured for background subtraction during the data analyses.

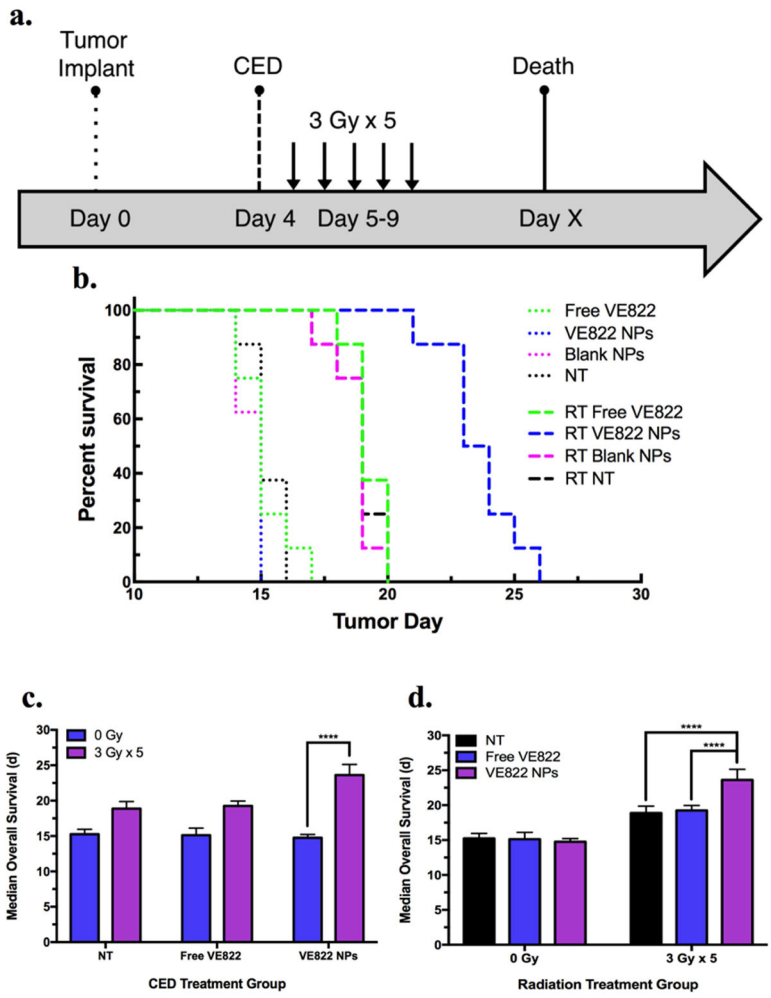

Figure 6. In vivo therapeutic efficacy

In vivo treatments of RG2 brain tumors in rats: (a) treatment course schematic. The dotted line indicates RG2 tumor cell infusion into the right caudate at day 0; the dashed line indicates intratumoral CED of either VE822-encapsulated P71D29 NP, free VE822, blank P71D29 NP or no treatment at day 4; the small arrows indicate administration of 5 consecutive doses of 3 Gy focal cranial radiation; the solid black line indicates the recorded survival of the treated animals. (b) *in vivo* survival study using RG2 rat glioma model in immunocompetent Fisher 344 rats. Kaplan Meier survival curves for different treatment groups of size n=8 are indicated. Group 1 (no RT): free VE822 (dotted-green), VE822 NPs (dotted-blue), blank NPs (dotted-purple), no treatment (NT, dotted-black). Group 2 (fractionated RT): free VE822 (dashed-green), VE822 NPs (dashed-blue), blank NPs (dashed-purple), no treatment (NT, dashed-black). (c) comparison of MOS among different CED treatment groups. (d) comparison of MOS among different radiation treatment groups. Data is shown as mean ± SEM (n=8). p-values were calculated as pair-wise log-rank comparisons from the survival curves and indicated as *<0.05, **<0.01, ***<0.005, ****<0.001.

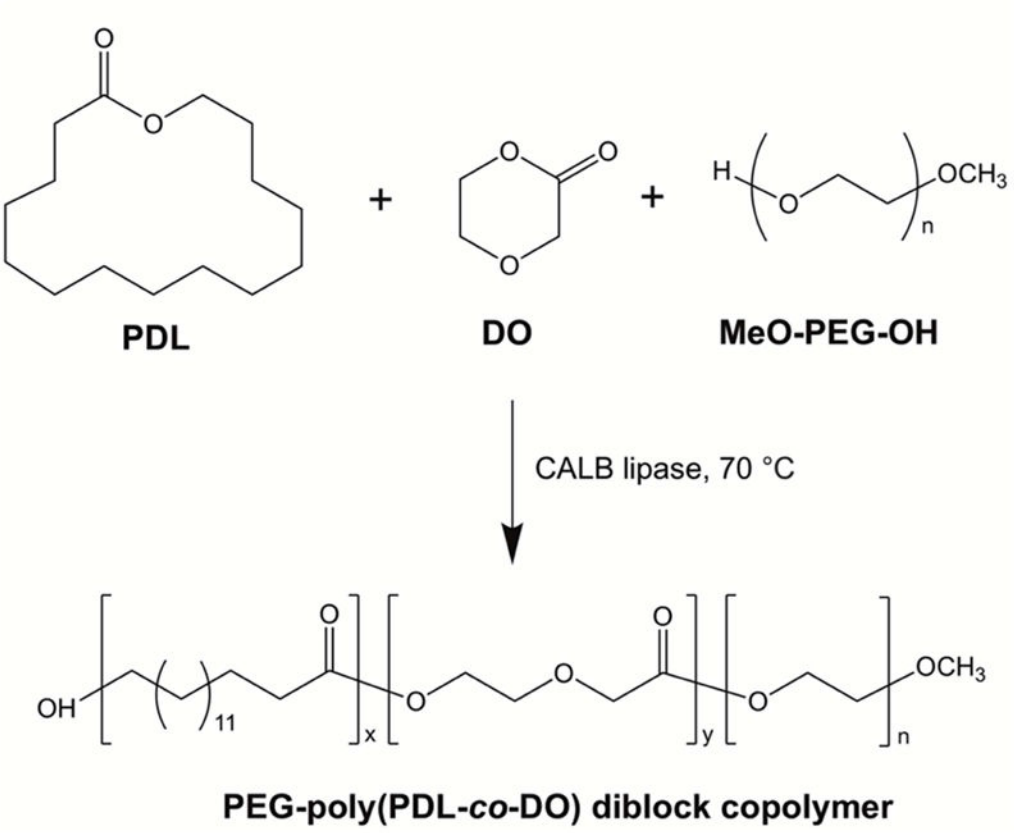

Scheme 1.
Enzymatic synthesis of PEG-poly(PDL-*co*-DO) block copolymers

Table 1

Analysis of PEG-poly(PDL-*co*-DO) diblock copolymers

Polymer	PDL/DO/PEG2K (feed molar ratio)	Polymer yield [a]	PDL/DO unit ratio (mol/mol)	PEG Content (wt%)	M_w (Da) [b]	M_w/M_n [b]
P56D44	40:60:4.2	71%	56:44	40%	12300	1.7
P65D35	50:50:4.6	72%	65:35	38%	13400	1.8
P71D29	60:40:5.0	77%	71:29	36%	15100	1.8

[a] Calculated based on total monomer substrate weight.

[b] Measured by GPC using polystyrene standards.

Table 2

Characterization of VE822-encapsulated PEG-poly(PDL-co-DO) nanoparticles

Polymer	Mean Hydrodynamic Diameter (nm)	Zeta Potential (mV)	Particle Yield (wt%)	Encapsulation Efficiency (%)	Encapsulation Amount (nmol/mg)
P56D44					
Blank	70±22.3	−17.4	60	-	-
Dye-loaded	78±25.6	−16.3	61	26±5.9	105±23.8
VE822-loaded	75±22.3	−15.4	60	25±4.7	101±19.0
P65D35					
Blank	86±19.8	−14.9	60	-	-
Dye-loaded	95±20.1	−12.6	56	34±7.6	136±30.6
VE822-loaded	90±19.8	−13.9	59	32±2.3	129±9.3
P71D29					
Blank	100±17.0	−16.2	63	-	-
Dye-loaded	105±14.9	−13.8	60	40±2.3	162±9.3
VE822-loaded	106±17.0	−14.2	57	42±3.5	170±14.1

Table 3

Drug release profiles of VE822 loaded PEG-poly(PDL-*co*-DO) NPs with drug release fit to exponential decay curves

Polymer	Burst Release (%)	Sustained release rate (nmol drug/mg NP/d)	Sustained release rate (% drug/d)
P56D44	29±1.3	0.8±0.1	0.8±0.1
P65D35	17±0.8	0.8±0.3	0.6±0.2
P71D29	9.1±3.3	1.0±0.2	0.6±0.1